Diffusion of Water in Clays on the Microscopic Scale: Modeling and Experiment

N. Malikova,*,†,‡ A. Cadène,† V. Marry,† E. Dubois,† and P. Turq†

Laboratoire Liquides Ioniques et Interfaces Chargées, boite postale 51, Université P. et M. Curie, 4 place Jussieu, F-75252 Paris Cedex 05, France, and ANDRA, Parc de la Croix Blanche, 1/7 rue Jean Monnet, F-92298 Châtenay-Malabry Cedex, France

Received: November 30, 2005; In Final Form: January 4, 2006

Diffusion of water in montmorillonite clays at low hydration has been studied on the microscopic scale by two quasi-elastic neutron scattering techniques, neutron spin−echo (NSE) and time-of-flight (TOF), and by classical microscopic simulation. Experiment and simulation are compared both directly on the level of intermediate scattering functions, $I(Q, t)$, and indirectly on the level of relaxation times after a model of atomic motion is applied. Regarding the dynamics of water in Na- and Cs-monohydrated montmorillonite samples, the simulation and NSE results show a very good agreement, both indicating diffusion coefficients of the order of $(1-3) \times 10^{-10}$ m^2 s^{-1}. The TOF technique significantly underestimates water relaxation times (therefore overestimates water dynamics), by a factor of up to 3 and 7 in the two systems, respectively, primarily due to insufficiently long correlation times being probed. In the case of the Na-bihydrated system, the TOF results are in closer agreement with the other two techniques (the techniques differ by a factor of 2−3 at most), giving diffusion coefficients of $(5-10) \times 10^{-10}$ m^2 s^{-1}. Attention has been also paid to the elastic incoherent structure factor, EISF(Q). Simulation has played a key role in understanding the various contributions to EISF(Q) in clay systems and in clearly distinguishing the signatures of "apparent" and true confinement. Indirectly, simulation highlights the difficulty in interpreting the EISF(Q) signal from powder clay samples used in experiments.

1. Introduction

Clay minerals are highly abundant constituents of soil, and the study of their physical/chemical properties is crucial for a vast range of phenomena, ranging from geological (soil stability) to biochemical (catalysis). Motivated by the potential use of clays in barriers around underground storage sites of radioactive waste, the current study deals with the mobility of water confined in clay minerals investigated on the microscopic scale by modeling (microscopic simulation) and experiment (quasi-elastic neutron scattering).

Clay minerals are layered aluminosilicates, with each layer consisting of fused sheets of octahedra of Al^{3+} or Mg^{2+} oxides and tetrahedra of Si^{4+} oxides.[1] Isomorphic substitutions of the metal atoms result in an overall negative charge on the individual clay layers, compensated by positive counterions between them (interlayers). The hydration of counterions, under increasing humidity, is the driving force for the incorporation of water between the clay layers, thus causing the system to swell. In the initial stages, discrete layers of water molecules are formed in the interlayer, referred to as monolayer, bilayer hydrates, and so forth.[2] These low hydration states are investigated here.

The dynamics of water in clays has been studied independently by both microscopic simulation[3−7] and quasi-elastic neutron scattering.[8−15] Both of these approaches study dynamics on the scale of picoseconds and nanometers and should be contrasted with abundant macroscopic diffusion studies of clays (tracer experiments)[16,17] (scale of hours, days, and meters) which stand aside and cannot be directly compared.

For the microscopic diffusion studies, the simulation−experiment comparison has been almost exclusively made on the level of diffusion coefficients. These are obtained from the analysis of particle trajectories (mean squared displacement, autocorrelation of velocity methods) for the case of simulations and the Q-dependence of relaxation times extracted from scattering functions ($I(Q, t)$, $S(Q, \omega)$) for the case of neutron scattering. The summary of diffusion coefficients for water in clays thus determined is available elsewhere.[18] However, the extent of averaging and approximation that the determination of a single value of a diffusion coefficient entails is rather detrimental and we concentrate here on a detailed comparison of the dynamic data obtained by neutron scattering and simulation; more specifically, we consider the intermediate scattering function, $I(Q, t)$, obtained by the various techniques. Further, we model the experimental and simulated signals in the low Q region with a simple model of isotropic continuous translation and extract the corresponding relaxation times. Last, we study the elastic incoherent structural factor, EISF(Q), and its interpretation in terms of confinement of diffusing scatterers. Following our previous publication,[18] we take the example of sodium montmorillonite in both mono- and bihydrated states and cesium montmorillonite in the monohydrated state.

2. Simulation Techniques

The simulation box consisted of two clay layers (area 20.72 Å × 17.94 Å, thickness 6.54 Å), with each being formed of eight unit cells of the formula $Na_{0.75}[Si_8](Al_{3.25}Mg_{0.75})O_{20}(OH)_4$ and its charge being balanced by six cations in the interlayer. The counterions considered were Cs^+ and Na^+, in the monohydrated and bihydrated (for Na^+ only) states corresponding to 6 and 12 water molecules per cation, respectively.[3] The

* Corresponding author. E-mail: malikova@ccr.jussieu.fr. Phone: 01 44 27 31 18. Fax: 01 44 27 32 28.
† Université P. et M. Curie.
‡ ANDRA.

10.1021/jp056954z CCC: $33.50
Published on Web 02/01/2006

dimensions of the overall simulation box (parallelopided) were $a = 20.72$ Å, $b = 17.94$ Å, $c = 24-30$ Å (depending on the hydration state), $\alpha = \gamma = 90°$, and $\beta \neq 90°$. Periodic boundary conditions were applied in all three directions. The interatomic potentials between each pair of atoms in the system were the Lennard-Jones and Coulombic potentials. Atomic charges and Lennard Jones parameters for each atom were taken from Smith et al.[19] for the clay and Berendsen et al.[20] for the model of water (SPC/E model). Both the clay layers and individual water molecules were considered here as rigid. Further details of this common model of clay systems can be found in previous simulation studies.[21−24]

After Monte Carlo simulations in the *NPT* ensemble were conducted to obtain equilibrium layer spacing for a given composition of the interlayer, molecular dynamics simulations (*NVE* ensemble, $t_{step} = 0.001$ ps) traced the motion of the interlayer cations and water, while the clay layers themselves were kept stationary. Coordinates of all mobile atoms were recorded every 0.02 ps throughout simulations of 655 ps in total length. The final data from molecular dynamics simulations are thus, for each atom, in the form of trajectories or time-dependent position, $\mathbf{R}(t)$.

The quantities calculated directly from the simulated particle trajectories were the incoherent intermediate scattering function, $I_{inc}(Q, t)$, and the elastic incoherent structural factor, EISF(Q), formally corresponding to $I_{inc}(Q, t)$ in the limit of $t \rightarrow \infty$. The corresponding formulas are

$$S_{inc}(Q, t) = \frac{1}{N_H}\sum_{\forall H}\overline{\langle \exp[-i\mathbf{Q}\cdot\mathbf{R}_H(0)]\, \exp[i\mathbf{Q}\cdot\mathbf{R}_H(t)]\rangle^Q} \quad (1)$$

$$\mathrm{EISF}(Q) = \frac{1}{N_H}\sum_{\forall H}\overline{\langle |\exp[-i\mathbf{Q}\cdot\mathbf{R}_H]|^2\rangle^Q} \quad (2)$$

Unless specified otherwise, at every value of Q and for each H atom separately, the average of the correlation function (notation $\overline{\langle ... \rangle^Q}$) was carried out over 10 Q vectors of the same modulus *isotropically* distributed in space. This type of averaging mimics the signal from a powder clay sample, that is, a sample in which the orientation of clay layers is isotropic, as was assumed to be the case for the real clay samples in the neutron scattering experiments. The above two simulated quantities shall be directly compared to their experimentally determined counterparts and later analyzed in terms of a specific model of atomic motion.

3. Experimental Techniques

Natural sodium montmorillonite was obtained by purification and homoionization of commercial bentonite MX-80. Bentonite (40 g) dispersed in deionized water (1 dm^3) was centrifuged (approximately 20 000 g for 30 min) and the top part of the sediment redispersed in deionized water (pH 5, 80 °C) by stirring (12 h). The extracted material was dispersed in 0.1 M NaCl or CsCl solution by stirring (12 h, two times), repeatedly washed (deionized water) until complete removal of Cl^- ions ($AgNO_3$ test), dried (at 80 °C over silica gel for a matter of days), and crushed, and the resulting powder was stored under a dried atmosphere. This procedure leads to a size fraction of <2 μm of montmorillonite particles. As determined by Guillaume et al.,[25] the resulting material is $Cat_{0.76}[Si_{7.96}Al_{0.04}](Al_{3.1}Mg_{0.56}Fe^{III}_{0.18}Fe^{II}_{0.16})O_{20}(OH)_4$, where Cat stands for the interlayer counterion, Na^+ or Cs^+ in this case. Dried purified samples were equilibrated (3 weeks) at the desired relative humidity (43 and 85−95% for Na-mono and Cs-mono/Na-bilayer, respectively) at 25 ± 2 °C. The water intake was monitored by mass measurements. Note that the above clay drying procedure results in residual water content in the "dry" sample, approximately 1 H_2O/counterion. Complete removal of interlayer water results in irreversible partial loss of rehydration properties of the clay.[26,27]

Neutron spin−echo (NSE)[28,29] and time-of-flight (TOF)[30] experiments were carried out on the MUSES and MIBEMOL spectrometers at LLB, Saclay, France. The montmorillonite samples were fully hydrogenated, and thus, to a good approximation, the incoherent scattering signal from the H atoms in the sample was monitored. For the NSE technique, polarization of the scattered neutron beam was measured under ambient pressure at carefully chosen Q values, between 0.5 and 1.8 $Å^{-1}$, in zones of no coherent contribution from the clay structure. By combination of both the NSE and neutron resonance spin−echo (NRSE) techniques,[31−33] measurements for correlation times up to approximately 500 ps were achieved. Time-of-flight measurements were carried out under reduced pressure (He 200 mbar) at an incident neutron wavelength of 9 Å (Q range 0.21−1.28 $Å^{-1}$, resolution (HWHM) 14 μeV).

While the NSE technique in the case of clay systems gives direct access to the incoherent intermediate scattering function, $I_{inc}(Q, t)$, the TOF technique measures the scattering function, $S_{inc}(Q, \omega)$, which is formally related to $I_{inc}(Q, t)$ by a Fourier transformation in time.

4. Theoretical Background—Models of Atomic Motion

For the interpretation of quasi-elastic neutron scattering signals using a given model of atomic motion, explicit functions representing atomic translation and rotation are necessary. In the low Q region, due to intensity considerations, the use of a single translational term tends to be a good approximation.[30] The high resolution TOF measurements allow analysis of the quasi-elastic zone in terms of translational motion without a rotational contribution not *only* due to a very low intensity of the transrotational term in the low Q region but also due to resolution considerations. More to the latter, a peak significantly broader than the energy transfer range accessible for analysis (as expected in the case of the transrotational term here) is seen as a flat background. For 9 Å incident neutrons on the MIBEMOL apparatus, the analysis range is −0.2 to +0.2 meV due to the cutoff in the energy loss side.

Taking the ideal case of an isotropic continuous translation, for which the van Hove self-correlation function, $G(R, t)$, is a Gaussian, the intermediate scattering function ($I(Q, t)$, measured quantity of the NSE technique) is an exponential and the scattering function ($S(Q, \omega)$, measured by the TOF technique) is a Lorentzian.[34] In real systems, however, we almost always find deviations from this ideal behavior. This applies for both experiment and simulation and is linked to the presence of several families of diffusing species with different relaxation times, the presence of an interface, and thus the breaking down of the isotropic nature of diffusion. A more general model for the low Q region, which allows for a range of relaxation times in the sample, comes (in the (Q, t) domain) in the form of a stretched exponential

$$I(Q, t) = A \exp[-(t/\tau)^\beta] + (1 - A), \quad \text{with } 0 < \beta \leq 1 \quad (3)$$

with both β and τ now as the fit parameters. The lower the coefficient β, the more severe departure from the monoexponential behavior is indicated. The average relaxation time at

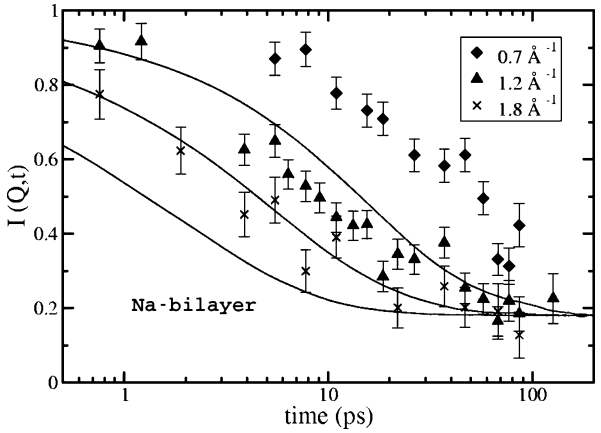

Figure 1. Intermediate scattering functions, $I(Q, t)$, from simulation (full lines) and neutron spin−echo experiments (symbols) for the Na-bilayer system. (Data for the sample equilibrated at 85% relative humidity are presented.)

each Q value is

$$\langle\tau\rangle = \frac{\tau}{\beta}\Gamma\left(\frac{1}{\beta}\right) \tag{4}$$

where Γ indicates the Gamma function, which has a known analytical form. The diffusion coefficient can then be extracted from the gradient of the plot of inverse average relaxation times versus Q^2, in the limit of $Q^2 \rightarrow 0$.

Note that for the NSE technique the resolution function of the apparatus simply multiplies the sample signal, and thus, after a division, we can deal directly with the "true" sample signal and model it using eq 3. In the case of the TOF technique, the resolution function cannot be eliminated as easily; the overall raw signal is, to a first approximation, a convolution of the true sample signal and the resolution function. The data treatment in the case of the TOF technique is thus more demanding and needs to include the resolution function explicitly. An analytical expression for the analogue of the stretched exponential ("stretched Lorentzian") does not exist. The modeled signal is generated and *modified* by the TOF resolution function in the (Q, t) domain, and the result is then Fourier transformed numerically into the (Q, ω) domain for comparison with the raw TOF sample data. This treatment is equivalent to modeling the raw TOF signal, $S'(Q, \omega)$, as

$$S'(Q, \omega) = [1 - A(Q)]\,\mathrm{Res}(\omega) + A(Q)[\mathrm{Res}(\omega) \otimes S^{\mathrm{model}}(Q, \omega)] \tag{5}$$

where $\mathrm{Res}(\omega)$ represents the TOF resolution function, $S^{\mathrm{model}}(Q, \omega)$ represents the Fourier transform of the stretched exponential, and $[1 - A(Q)]$ and $A(Q)$ represent the normalized intensities of the elastic and quasi-elastic scattering contributions, respectively.

5. Results and Discussion

5.1. Direct Comparison in the (*Q, t*) Domain. In this section, we compare at first the incoherent intermediate scattering functions, $I_{\mathrm{inc}}(Q, t)$, as measured by the NSE technique and their simulated counterparts. Second, we attempt a transformation of the TOF data into the (Q, t) domain for direct comparison with the other two techniques.

Figures 1 and 2 compare directly the simulated and experimental (NSE) intermediate scattering functions for the three systems studied, in each case for three Q values, as indicated. Simulation predicts decreasing relaxation times (faster dynamics)

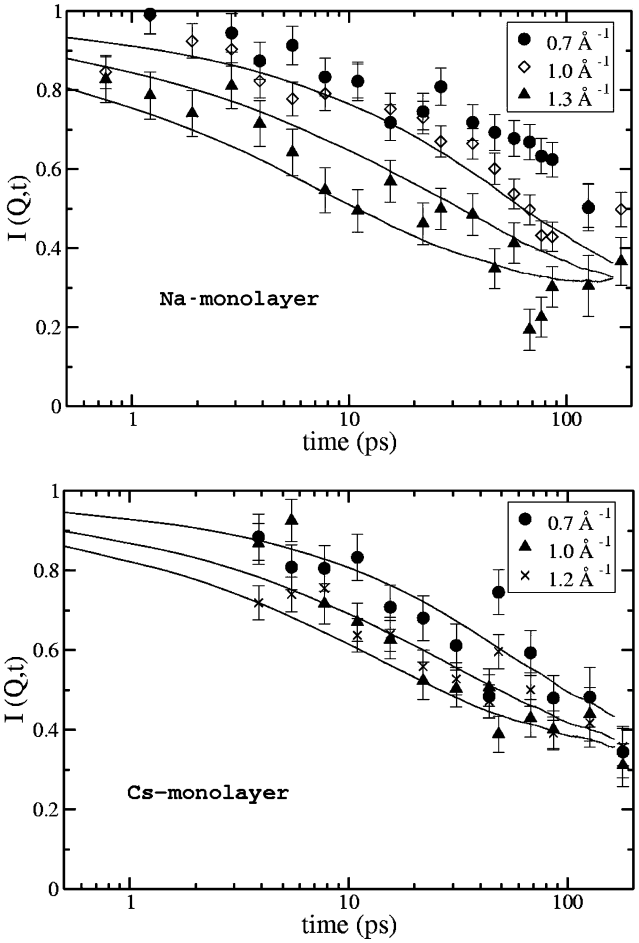

Figure 2. Intermediate scattering functions, $I(Q, t)$, from simulation (full lines) and neutron spin−echo experiments (symbols) for the Na- and Cs-monolayer systems.

in the order of Cs-monolayer, Na-monolayer, and Na-bilayer. In the NSE technique, the difference between the two monolayers is marginal, but clearly, faster dynamics is seen for the Na-bilayer. The agreement between the two methods is very good in the case of monolayers. Nevertheless, the simulation results are shifted slightly toward lower relaxation times (faster dynamics). This difference is accentuated in the bilayer state (difference reaching a factor of approximately 2−3 between the experimental and relaxation times). Note that all of the NSE signals decay to a nonzero background constant, which corresponds to the percentage of immobile H atoms in the system (structural OH groups in clay layers). This is approximately 20% in the Na-bilayer and 30% in the monohydrated systems. It is interesting to note here that the ion diffusion, as seen by microscopic simulation, is very different for the two counterions considered (in monohydrated systems).[6] While Cs^+ ions show clear site-to-site jump diffusion between so-called trigonal sites, the diffusion of Na^+ ions is rather delocalized with the absence of any clear preferential sites. Also, by simulation, the behavior of the water phase was seen to be similar in the two systems,[6] which agrees with the current NSE data for water diffusion.

For any meaningful comparison of the dynamics observed, the water contents in the simulated and experimental samples should be close. The simulated water contents are based on a previous simulation study,[3] which showed that they reproduce the experimentally observed interlayer spacing of montmorillonite clay samples, *as determined from the position of the 001 reflection in X-ray diffractograms* for a given relative humidity.[35−37] The total water content in a real clay sample,

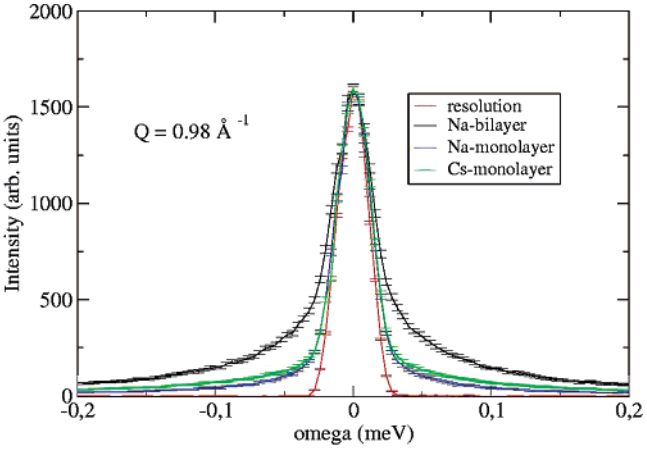

Figure 3. Examples of raw TOF data (in the (Q, ω) domain) for all three systems studied together with the TOF resolution function.

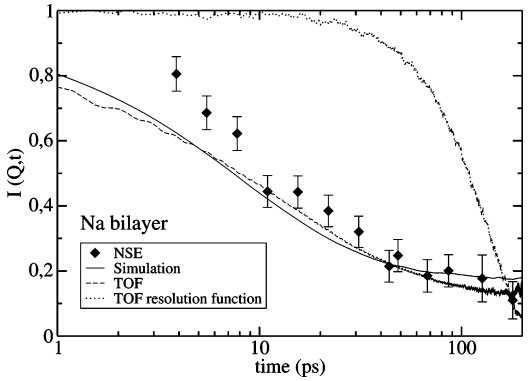

Figure 4. Direct comparison of TOF, NSE, and simulation data in the (Q, t) domain. The example shown is of the Na-bilayer system and data at $Q \simeq 1.0$ Å^{-1}.

determined by mass measurements, for instance, is subject to uncertainty partly due to problems of hysteresis in clay hydration but also due to uncertainty of residual water content in dry clay samples that are taken as the initial reference state. As mentioned earlier, complete removal of water from the system is detrimental. These cannot ever be truly dehydrated, as complete removal of water from the interlayer irreversibly destroys the rehydration properties of the system.[26,38] A rather complex picture of clay hydration emerges when a detailed analysis of X-ray diffractograms of real clay systems is considered,[39,40] pointing toward the coexistence of mono- and bihydrated states at a given relative humidity. There is even evidence for a variable water content at a given interlayer spacing.[41] Both phenomena are linked, for example, to local charge inhomogeneities on clay layers, always present in natural clays. Therefore, even if the overall simulated and experimental water contents coincide well, the distribution of water in individual interlayers of the real clay system is likely to vary. The current model clay system on the other hand is restricted to identical water contents in each interlayer (and homogeneous charge distribution on the clay layers). In this respect, it is not surprising to find some differences between the simulated and experimentally observed dynamics. At first sight, it could be the highest water content in the Na-bilayer sample, with the highest number of possible water redistributions, accounting for the greatest simulation−experiment difference.

Adding the results of the TOF technique, Figure 3 gives an example of the raw TOF data, in the (Q, ω) domain, for all three systems studied at $Q = 1$ Å^{-1}. In general, the wider the quasi-elastic broadening observed (as compared to the width of the resolution function), the faster the dynamics probed. As in the case of the NSE technique, the TOF raw data suggests only a marginal difference between the two monolayer systems while it shows clearly faster dynamics in the Na-bilayer.

Returning to the issue of direct comparison of NSE, TOF, and simulation data, two possibilities exist. On one hand, this can be done in the (Q, ω) domain into which the simulated and treated NSE data are transformed and modified by the TOF resolution function for direct comparison with the raw TOF sample data, such as the ones shown in Figure 3. On the other hand, the comparison can be made in the (Q, t) domain, into which the TOF data are transformed with the elimination of the TOF resolution function (by division). The TOF true sample signal is then compared with NSE and simulation data such as those in Figures 1 and 2.[42,43]

Both of the above transformation paths have weak points. The former path, taking the simulated and already treated NSE data and convoluting them with the TOF resolution function, amounts to a further degradation of the signals themselves. The latter path suffers from deformations during the inverse Fourier transforms of the raw sample data due to the proximity of the cutoff of the measured positive energy transfers to the elastic peak (becomes more serious with increasing Q due to increasing broadening of the quasi-elastic signal) as well as uncertainty in the normalization factors (values at $t = 0$) of the resulting $I(Q, t)$ signals.[43]

Overall, it is not obvious which of the above transformation paths is preferable. We present here the second path for the Na-bilayer system for a wave vector of 1.0 Å^{-1}. (It was necessary to extrapolate the raw TOF $S(Q, \omega)$ signal into large positive energy transfers (symmetric extrapolation around $\omega = 0$) prior to the inverse Fourier transformation in order to eliminate "ringing" phenomena in the resulting (Q, t) signal.[44]) The final TOF signal in the (Q, t) domain is shown in Figure 4 together with the simulated and NSE data as well as the TOF resolution function in the (Q, t) domain. (We performed a check to ensure that the variations of the resolution function as a function of energy transfers can be neglected for this system; i.e., quasi-elastic broadening is sufficiently small. As a result, the raw TOF signal can indeed be well approximated by a convolution between the resolution function and the true sample signal and thus the resolution *can* be eliminated by a simple division in the (Q, t) domain.)

From Figure 4, TOF data appear very close to the simulation, while both show faster dynamics than the NSE data. This shall be confirmed, for the wave vector chosen, in the following section in which all three types of data are analyzed in terms of a model of atomic motion and the corresponding relaxation times. The comparison of extracted relaxation times from the raw TOF (Q, ω) data and the transformed TOF data in the (Q, t) domain serves indirectly as a test for the validity of the transformation. The transformed TOF data from the monolayer systems did *not* "pass" this test. We suspect it is due to the very narrow quasi-elastic broadening compared to the resolution function seen for these systems, which introduced significant errors in the $\omega \rightarrow t$ transformation (involves division of the raw signal by the resolution).

5.2. Comparison on the Level of Relaxation Times. In this section, we depart from the *stretched* exponential form characteristic of the continuous isotropic translation, fit the experimental and simulated data, up to wave vectors of approximately 1.2 Å^{-1}, and extract the corresponding relaxation times. The fitting procedure was performed over the time range 1−300 ps for simulation and the NSE technique and over the energy range from −0.2 to 0.2 meV for the TOF technique. The plots of

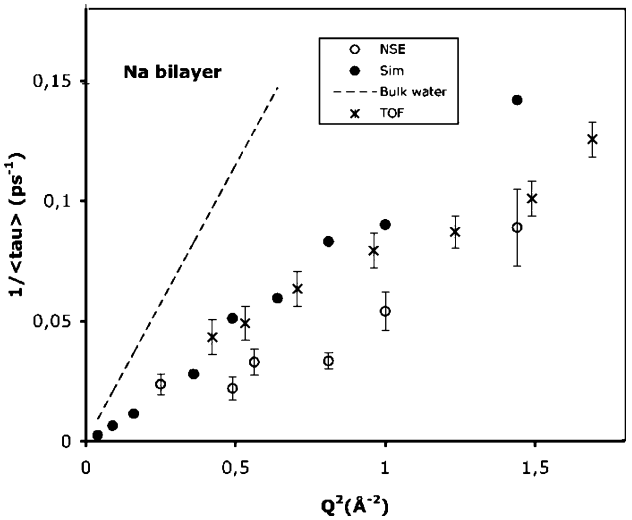

Figure 5. Plot of $1/\langle\tau\rangle$ versus Q^2 in the low Q range for the Na-bilayer system.

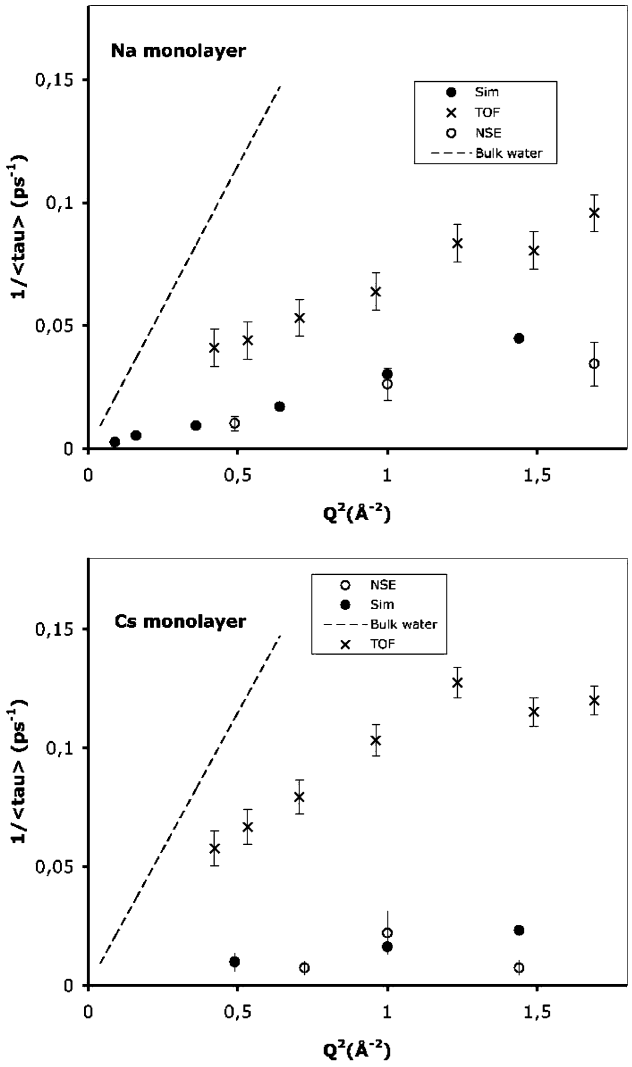

Figure 6. Plot of $1/\langle\tau\rangle$ versus Q^2 in the low Q range for the Na- and Cs-monolayer systems.

$1/\langle\tau\rangle$ versus Q^2 corresponding to the three systems studied are summarized in Figures 5 and 6. Note that, with increasing Q, β exponents decreased down to 0.5, indicating a severe departure from monoexponential behavior. This was true for both simulated and experimental data sets.

Regarding the simulation−experiment comparison, in the bilayer state, the TOF technique and simulation show somewhat faster dynamics than the NSE technique itself, as was already seen from the direct comparison. On the other hand, for the monolayer systems, the NSE technique and simulation are in very good agreement (consistent with direct comparison), while TOF measurements indicate considerably faster dynamics in both monolayer states. While the TOF data for the bilayer state are consistent with diffusion coefficients from previous TOF studies, this is not the case for the monolayer data; the current TOF data show significantly faster dynamics.[8,10,11] At this point, it is very instructive to mention the range of correlation times available with the three techniques. While simulation and the NSE technique can probe correlation times up to approximately 300−500 ps, for the TOF technique, the cutoff comes much earlier, around 70−100 ps. Comparing Figure 4 which features the TOF resolution function in the (Q, t) domain for the apparatus used and Figure 2 showing the decay of the signals from the three clay systems as seen by the NSE technique, the TOF resolution function decays faster than the NSE sample signals. In other words, a proportion of slow moving H atoms (relaxation times beyond 70−100 ps), significant especially for the monohydrated systems, will be seen as immobile by the TOF technique. These H atoms contribute to elastically scattered intensity (scattering with zero energy transfer) and are excluded from the dynamical analysis, shifting the overall relaxation times to lower values, that is, faster dynamics. In addition, the effect of this low TOF resolution cutoff is more pronounced with decreasing Q, as the signals decay slower (low Q region important for the determination of diffusion coefficients). Note that the extracted average relaxation times for the Cs-monolayer system are most certainly an underestimate, as the raw TOF data (see Figure 3) show clearly slower dynamics in the Cs-monolayer than the Na-bilayer. The extracted average relaxation times are shorter (faster dynamics) for the Cs-monolayer than for the Na-bilayer, pointing toward a problem in the model fitting.

In summary, the agreement between NSE and simulated data for the monohydrated systems is very good, as was already indicated by the direct comparison of $I(Q, t)$ signals. The faster dynamics indicated by TOF data is a consequence of the insufficiently long correlation times probed. Following the reasoning of accessible correlation times for the three techniques, for the Na-bilayer system, we would expect a very good agreement between NSE, simulation, *and* TOF data, as the times probed by the TOF technique seem to be sufficiently long for the relaxation of all of the mobile H atoms in the interlayer of this system. However, we see a difference of up to a factor of 2−3 in the relaxation times between the TOF (agrees well with simulation) and NSE data. Remembering the problem of a variable water content in the real clay system, interstratification, the complexity of the experimental techniques, and so forth, the agreement to within a factor of 2−3 could just as well be treated as a success. The crucial test would be comparing TOF and NSE measurements from the same, *physically* the same, clay sample to avoid any potential difference in hydration states.

We recognize that isotropic continuous translation, as applied in this section, might appear as a rather crude model for the diffusion of water in the clay interlayer. A number of TOF studies on bulk supercooled water,[45,46] confined water,[47,48] and clays themselves[8,10,11] support the isotropic jump translation model. Agreement has however not been reached between TOF studies and simulation on the applicability of this model to water in the bulk state at low temperatures,[49] and in more complex

systems such as polymer solutions[50] and clays.[51,52] For a convincing argument in favor of the jump rather than continuous translational diffusion, reliable data for high Q values are necessary, as this is the regime in which the two models diverge (a plateau appears in the plots of $1/\langle\tau\rangle$ versus Q^2 for jump diffusion).[30] The high Q region is however also the region where trans-rotational coupling becomes significant and thus modeling with a single translational term (continuous or jump) is insufficient. Previous studies have used without exception the model for rotation on a sphere when incorporating the trans-rotational term. We feel that this choice is not obvious, as preferential orientations of water molecules in the low hydrated clay interlayer are very probable[4,6,53] and the rotation is likely to be restricted. From the data sets available to us under this study and above all using the analysis with a purely translational model, we cannot conclude for or against jump diffusion. We are in the process of developing, with the aid of microscopic simulation, a refined model for the rotational motion of water molecules in the clay interlayer.

A second issue is concerned with the *isotropic* nature of the translational diffusion of water in clays. The more appropriate model seems to be that of the isotropically averaged two-dimensional translational diffusion. As discussed in detail by Lechner et al.,[54] the signal from isotropically averaged 2D diffusion differs only slightly from the isotropic diffusion in the quasi-elastic broadening, with the main difference being in the intensity at zero energy transfers (i.e., elastic contribution). In indirect agreement with this, for example, the decay of our NSE experimental data can be equally well fitted with the isotropic and powder-averaged 2D model. In other words, the experimental error bars are too large to distinguish the two models. The application of the significantly more complex averaged 2D model thus brings no additional information.

5.3. Elastic Incoherent Structure Factor. In the previous sections, we discussed the dynamic information extracted from the decay of the intermediate scattering functions, $I(Q, t)$, or broadening of the scattering functions, $S(Q, \omega)$. We noted that, for a given scattering wave vector, Q, scatterers seen as immobile *on the space and time scales of the measurements* (note that the time scale of measurements is always limited, by the resolution of the experimental setup or the length of a simulation) contribute to a constant background in $I(Q, t)$ and to intensity at zero energy transfers (i.e., elastic peak intensity) in $S(Q, \omega)$. In this section, we look in more detail at the percentage of immobile scatterers seen at different values of Q or the elastic incoherent structure factor, EISF(Q). As shall be seen, this *static* quantity can give information on the geometry of confining media in which scatterers diffuse.

For the NSE method, EISF(Q) has been taken simply as the long-time value of the intermediate scattering function at a given value of Q. In the case of simulation, EISF(Q) has been calculated according to eq 2, which for long simulation times is equivalent to taking the long-time value of $I(Q, t)$ calculated according to eq 1. For the TOF technique, EISF(Q) is the ratio of the elastic and total (elastic + quasi-elastic) scattered intensities at a given value of Q, that is, $[1 - A(Q)]$ as used in eq 5. Figures 7 and 8 summarize the EISF(Q) for all three systems studied by the NSE technique, the TOF technique, and simulation. These are the results of an isotropic analysis, that is, average over Q vectors isotropically distributed in space (refer back to eq 2 for the case of simulation).

For the Na-bilayer, the agreement of the three methods is very good in the range shown; down to $Q = 0.7$ Å^{-1}, the three sets do not show any increase with respect to an expected

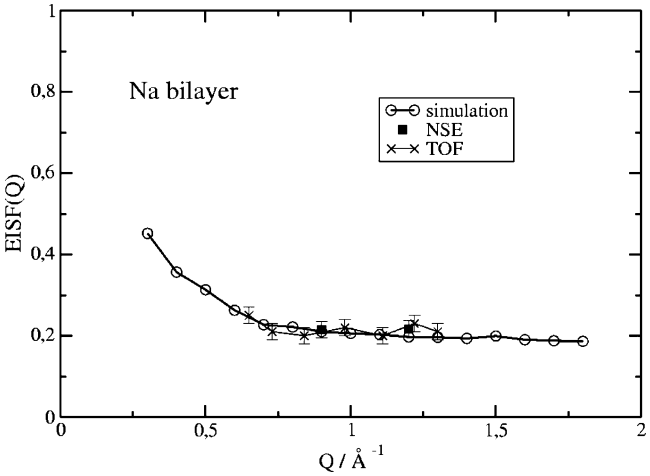

Figure 7. Elastic incoherent structure factor for the Na-bilayer system determined by the NSE technique, the TOF technique, and simulation (isotropic calculation in the case of simulation).

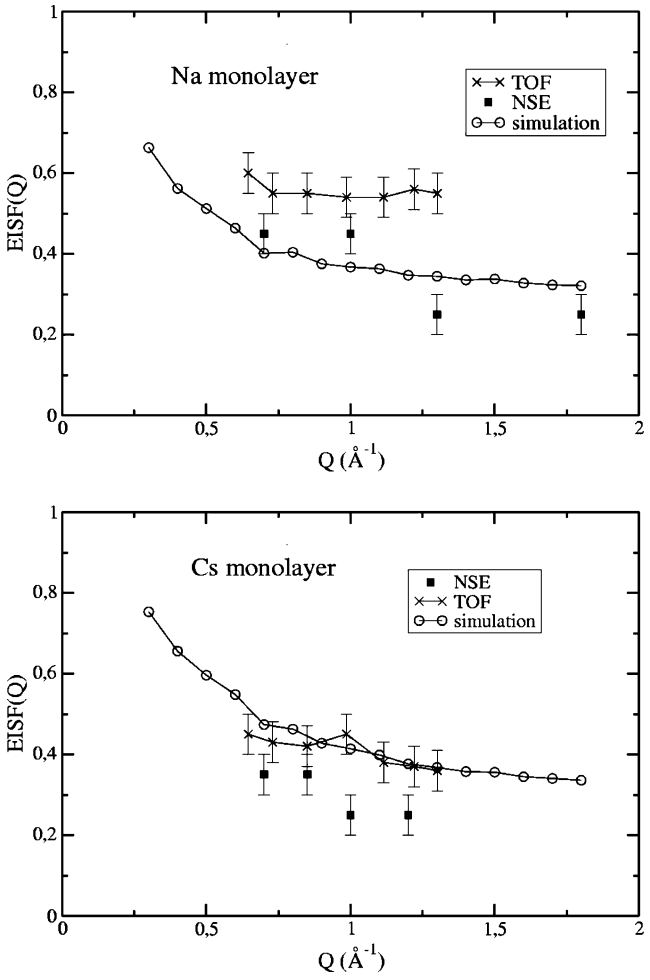

Figure 8. Elastic incoherent structure factor, EISF(Q), for the Na- and Cs-monolayer systems determined by the NSE technique, the TOF technique, and simulation (isotropic calculation in the case of simulation).

constant background corresponding to immobile structural H atoms. (Note that there is no contradiction in obtaining a very close agreement in the EISF(Q) from simulation and the NSE technique as well as relaxation times that are different by a factor of 2−3. While the latter is concerned with the decay of the $I(Q, t)$ signals, the former is only related to their long-time plateau.) Below $Q = 0.7$ Å^{-1}, the simulated data show an

upward trend; unfortunately, in this low Q region, no experimental data are available. The results for the monolayer states are at first sight much less satisfactory. Regarding the simulated data for both monolayer systems, it appears higher than the expected constant background corresponding to the structural H atoms (around 30%). Comparing then the two sets of experimental data, we note that in both monolayer systems the TOF set is higher than the NSE counterpart. If we assume that the experimental samples in the two cases had the same water content (though note that physically different samples were used and some differences are thus inevitable and shall be accentuated in the normalized EISF signal), this observation is consistent with the conclusion of the previous section: due to very narrow broadening of the quasi-elastic signal with respect to the TOF resolution, the TOF technique overestimates the elastic intensity (and thus EISF(Q)) and as a result underestimates the relaxation times (predicts faster dynamics). The raw TOF sample data can be fitted, for the monolayer states, with a wide range of ratios for the intensities of the elastic and quasi-elastic peaks, as their respective broadenings become almost indistinguishable. The error bars on the resulting EISF(Q) are very difficult to determine.

Viewing the increase of EISF(Q) as Q decreases, seen for both the simulated and experimental data sets in at least some of the three samples, what is the underlying interpretation? Is it a signature of a real *spatial* confinement of the interlayer H atoms, or is it an "apparent" confinement arising simply due to an insufficient *time* scale probed, just like the reasoning behind the TOF data sets for monolayer systems lying higher than the NSE data sets? Concentrating from now on on the simulated EISF(Q) and the Na-bilayer system, we show how decoupling the motion of interlayer H atoms in the plane of the clay layers (plane *XY*, no spatial confinement) and in the direction perpendicular to them (*Z*, direction of spatial confinement) serves to distinguish the features of the apparent and true (spatial) confinement seen for the clay systems.

Figure 9 summarizes simulated EISF(Q) data determined from particle trajectories using eq 2, where the average over Q vectors was carried out either over 10 Q vectors distributed in the *XY* plane or 1 Q vector in the *Z* direction. In each case, the results of simulations of three different lengths are shown. The *XY* analysis gives us a very similar signal to the isotropic analysis; the overall shape is a gradual increase of the EISF(Q_{XY}) as Q decreases. As the interlayer H atoms are not spatially confined in their motion in the *XY* plane, this increase is purely an apparent confinement arising from insufficient simulation times. The asymptote as the simulation time tends to infinity is the constant background corresponding to the percentage of structural H atoms. Analysis along the *Z* direction shows a very different behavior. In this direction, interlayer H atoms are confined between two parallel plates separated by a distance, L, and as has been well established,[55,56] the predicted *one-dimensional* EISF(Q_Z) signal is of the form

$$\mathrm{EISF}(Q_Z L) = \frac{2}{(Q_Z L)^2}(1 - \cos(Q_Z L)) \qquad (6)$$

As seen from the best fit of the above analytical form to the EISF(Q_Z) for the three simulation lengths, the following can be concluded. Under a certain critical length (for the bihydrated system, it was 720 ps), the EISF(Q_Z) does not resemble the above analytical form, as the time is insufficient for the H atoms to explore fully the space available in the *Z* direction (feature of apparent confinement). As the length of the simulation

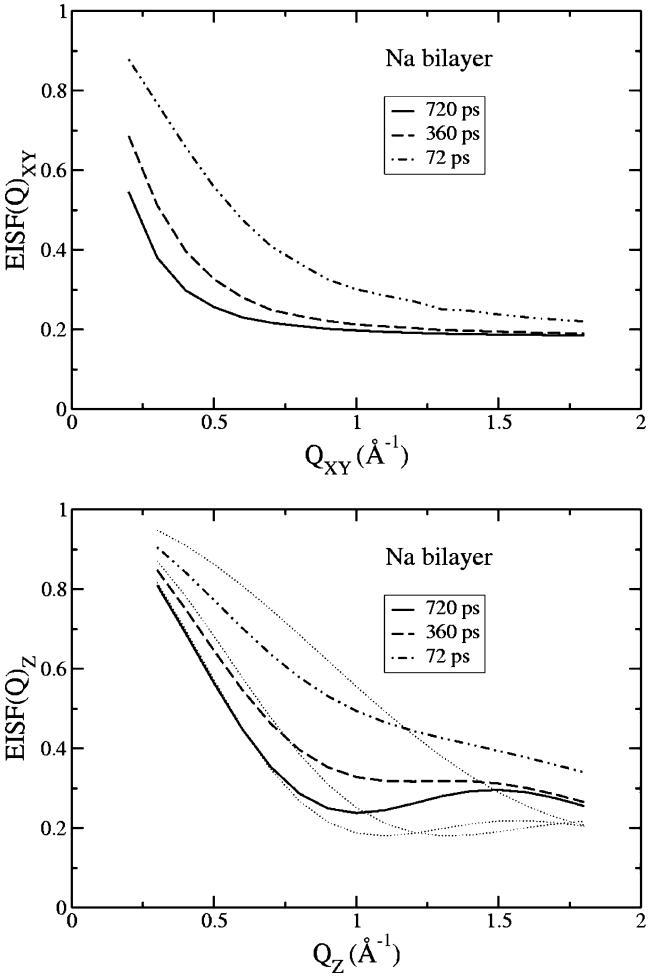

Figure 9. Influence of simulation time on the observed EISF(Q) signal both in the plane of the clay layers (*XY*), top, and in the direction perpendicular to them (*Z*), bottom. Example of the Na-bilayer system. The dotted lines in the bottom plot trace the best fits of a Bessel function form to the three EISF(Q) signals. The simulated EISF(Q) is clearly far from a Bessel function form for short simulations and approaches it as the simulation time is increased.

increases, the EISF(Q_Z) decreases to the above form (feature of true spatial confinement). The above analytical form *is* the asymptote of the EISF(Q_Z) signal as the simulation length tends to infinity, contrary to the background constant in the *XY* analysis. Furthermore, fitting the EISF(Q_Z) data of the longest simulation for all three clay systems studied, we arrive at realistic plate (clay layer) separations of 5.74, 2.79, and 2.83 Å for Na-bi, Na-mono, and Cs-monohydrate, respectively. This corresponds very well to the vertical space that H atoms explore during the simulation.[6]

Returning back to the interpretation of the EISF(Q) from isotropic analysis (both simulation and experiment), it is evident that features of both the apparent and true confinement are mixed. Detailed interpretation of the signal in terms of the dimension of confinement is therefore next to impossible. In addition, the limited set of experimental data, especially NSE, makes the fitting by a complex function rather meaningless.

6. Conclusion

Regarding the dynamics of water in Na- and Cs-monohydrated montmorillonite samples, the simulation and NSE results show a very good agreement, both indicating diffusion coefficients of the order of $(1-3) \times 10^{-10}$ m^2 s^{-1}. The TOF technique has been seen to significantly underestimate water

relaxation times (therefore overestimate water dynamics, by a factor of up to 3 and 7 in the two systems, respectively), primarily due to insufficiently long correlation times being probed.

In the case of the Na-bihydrated system, the TOF results are in closer agreement with the other two techniques (the techniques differ by a factor of 2−3 at most). The very close agreement between the NSE technique and simulation seen in the monohydrated systems is lost in the case of the Na-bilayer (evident especially in the direct simulation−NSE comparison in the (Q, t) domain). Both the simulation and TOF data yield a diffusion coefficient of approximately 10×10^{-10} m^2 s^{-1} (almost half of the bulk water diffusion coefficient), while the NSE data give approximately 5×10^{-10} m^2 s^{-1}. The water dynamics in this system is faster than that in the monohydrated counterparts, and the cutoff of measurable correlation times in TOF is less of a problem. To test whether an even closer agreement between the two experimental techniques can be achieved, the use of the same, physically the same, clay sample is perhaps the only solution, considering the complexity of the clay system and the inevitable variations of water contents between different clay samples.

As discussed previously, the simulated and experimental water contents in the clay samples are not easily matched, mainly due to uncertainties in the experimental water content determination using the traditional methods such as mass uptake used here. Even if the total water contents are matched, the redistribution of water in various interlayers (or porosities) in the real clay is likely to be nonuniform, contrary to what is used in the model clay. In this respect, we are satisfied to find an overall agreement within a factor of 2−3 between the simulated and experimental (NSE for all three systems and TOF for the bilayer system) data.

We have also presented a transformation of the raw TOF data into the (Q, t) domain for direct comparison with NSE and simulation data. This procedure is not straightforward, but we feel that the model fitting procedures that serve to extract relaxation times match it in complexity, especially for the TOF technique. This direct comparison of raw data from the NSE and TOF methods seems to be an important consistency check, prior to any model fitting being applied, and yet, it is explored only very rarely.

Apart from the study of dynamics, attention has been paid to the elastic incoherent structure factor, EISF(Q). Due to the one-dimensional nature of confinement in clays and the use of powder clay samples, the analysis of experimentally observed (isotropically averaged) EISF(Q) is not straightforward. Simulation has played a key role in understanding the various contributions to EISF(Q) in clay systems and in clearly distinguishing the signatures of apparent and true confinement.

As discussed in our previous paper,[18] the exploitation of more homogeneous or structurally less complex members of the clay family, such as hectorite or vermiculite, and a detailed characterization of their hydration states, is seen as necessary for advancement in the comparison of real and simulated dynamics and is currently underway for the hectorite system.

Acknowledgment. N.M. gratefully acknowledges the support of ANDRA (Agence Nationale pour la Gestion des Déchets Radioactifs). We also thank J.-M. Zanotti and S. Longeville for many discussions.

References and Notes

(1) Wyckoff, R. W. G. *Crystal Structures*; John Wiley and Sons: 1968; Vol. 4.
(2) Giese, R. F.; van Oss, C. J. *Surfactant Science Series*; Marcel Dekker: 2002; Vol. 105.
(3) Marry, V.; Turq, P. *J. Chem. Phys.* **2002**, *117*, 3454−3463.
(4) Chang, F. C.; Skipper, N. T.; Sposito, G. *Langmuir* **1995**, *11*, 2734−2741.
(5) Sutton, R.; Sposito, G. *J. Colloid Interface Sci.* **2001**, *237*, 174−184.
(6) Malikova, N.; Marry, V.; Dufrêche, J.-F.; Simon, C.; Turq, P.; Giffaut, E. *Mol. Phys.* **2004**, *102*, 1965−1977.
(7) Malikova, N.; Marry, V.; Dufrêche, J.-F.; Turq, P. *Curr. Opin. Colloid Interface Sci.* **2004**, *9*, 124−127.
(8) Cebula, D. J.; Thomas, R. K.; White, J. W. *Clays Clay Miner.* **1981**, *29*, 241−248.
(9) Poinsignon, C.; Estrade-Szwarckopf, J.; Conard, J.; Dianoux, A. J. *Proc. Int. Clay Conf. − Denver 1985* **1987**, 284−291.
(10) Tuck, J. J.; Hall, P. L.; Hayes, M. H. B.; Ross, D. K.; Hayter, J. B. *J. Chem. Soc., Faraday Trans. 1* **1985**, *81*, 833−846.
(11) Tuck, J. J.; Hall, P. L.; Hayes, M. H. B.; Ross, D. K.; Poinsignon, C. *J. Chem. Soc., Faraday Trans. 1* **1984**, *80*, 309−324.
(12) Swenson, J.; Bergman, R.; Howells, W. S. *J. Chem. Phys.* **2000**, *113*, 2873−2879.
(13) Swenson, J.; Bergman, R.; Longeville, S. *J. Chem. Phys.* **2001**, *115*, 11299−11305.
(14) Mamontov, E. *J. Chem. Phys.* **2004**, *121*, 9193−9194.
(15) Swenson, J.; Bergman, R.; Howells, W. S.; Longeville, S. *J. Chem. Phys.* **2004**, *121*, 9195.
(16) Molera, M.; Eriksen, T. *Radiochim. Acta* **2004**, *90*, 753−760.
(17) Daqing, C.; Eriksen, T. *Radiochi,. Acta* **1998**, *82*, 287−292.
(18) Malikova, N.; Cadene, A.; Marry, V.; Dubois, E.; Turq, P.; Zanotti, J.-M.; Longeville, S. *Chem. Phys.* **2005**, *317*, 226−235.
(19) Smith, D. *Langmuir* **1998**, *14*, 5959−5967.
(20) Berendsen, H. J. C.; Grigera, J. R.; Straatsma, T. P. *J. Phys. Chem.* **1987**, *91*, 6269−6271.
(21) Delville, A. *Langmuir* **1992**, *8*, 1796−1805.
(22) Boek, E. S.; Coveney, P. V.; Skipper, N. T. *Langmuir* **1995**, *11*, 4629−4631.
(23) Chang, F. C.; Skipper, N. T.; Sposito, G. *Langmuir* **1997**, *13*, 2074−2082.
(24) Chávez-Páez, M.; dePablo, L.; dePablo, J. J. *J. Chem. Phys.* **2001**, *114* (24), 10948−10953.
(25) Guillaume, D.; Neaman, A.; Cathelineau, M.; Mosser-Ruck, R.; Peiffert, C.; Abdelmoula, M.; Dubessy, J.; Villieras, F.; Baronnet, A.; Michau, N. *Clay Miner.* **2003**, *38* (3), 281−302.
(26) Fowden, L., Barrer, R. M., Tinker, P. B., Eds. *Clay Minerals: Their structure, behaviour and use*; Royal Society: London, 1984.
(27) Bérend, I. Les Mechanismes d'hydratation de montmorillonites homoioniques pour des pressions relatives inferieures a 0.95. These de doctorat, Institut National Polytechnique de Lorraine, 1991.
(28) Mezei, F. *Z. Phys.* **1972**, *255*, 146−160.
(29) Mezei, F. *Lecture Notes in Physics*; Springer-Verlag: 1980; Vol. 128.
(30) Bée, M. *Quasi-elastic neutron scattering; Principles and Applications in Solid State Chemistry, Biology and Material Science*; Adam Hilger: 1988.
(31) Golub, R.; Gahler, R. *Phys. Lett. A* **1987**, *123*, 43−48.
(32) Gahler, R.; Golub, R. *Z. Phys. B: Condens. Matter* **1987**, *65*, 269−273.
(33) Gahler, R.; Golub, R. *J. Phys. (Paris)* **1988**, *49*, 1195−1202.
(34) Hansen, J. P.; McDonald, I. R. *Theory of simple liquids*; Academic Press: 1986.
(35) Bérend, I.; Cases, J. M.; Francois, M.; Uriot, J. P.; Michot, L. J.; Masion, A.; Thomas, F. *Clays Clay Miner.* **1995**, *43*, 324−336.
(36) Cases, J. M.; Bérend, I.; Francois, M.; Uriot, J. P.; Thomas, F.; Poirier, J. E. *Langmuir* **1992**, *8*, 2730−2739.
(37) Cases, J. M.; Bérend, I.; Francois, M.; Uriot, J. P.; Michot, L. J.; Thomas, F. *Clays Clay Miner.* **1997**, *45*, 8−22.
(38) ANDRA. *Referentiel Materiaux, Tome 2: Les Materiaux argileux*; Rapport C.RP.AMAT.01.060, 2001.
(39) Weaver, C. E. *Am. Mineral.* **1956**, *41*, 202−221.
(40) Ferrage, E.; Lanson, B.; Sakharov, B. A.; Drits, V. A. *Am. Mineral.* **2005**, *90*, 1358−1374.
(41) Michot, L. J.; Villiéras, F.; François, M.; Bihannic, I.; Pelletier, M.; Cases, J. M. *C. R. Geosci.* **2002**, *334*, 611−631.
(42) Howells, W. S. *Physica B* **1996**, *226*, 778−81.
(43) Trouw, F.; Bedrov, D.; Borodin, O.; Smith, G. D. *Chem. Phys.* **2000**, *261*, 137−148.
(44) Press, W. H.; Flannery, B. P.; Teukolsky, S. A.; Vetterling, W. T. *Numerical Recipes, The Art of Scientific Computing*; Cambridge University Press: 1986.
(45) Teixeira, J.; Bellissent-Funel, M.-C.; Chen, S.-H.; Dianoux, A. J. *J. Phys.* **1984**, *C7*, 65−71.
(46) Bellissent-Funel, M.-C.; Teixeira, J. *J. Mol. Struct.* **1991**, *250*, 213−230.

(47) Bellissent-Funel, M.-C.; Bradley, K. F.; Chen, S.-H.; Lal, J.; Teixeira, J. *Physica A* **1993**, *201*, 277−285.
(48) Teixeira, J.; Zanotti, J.-M.; Bellissent-Funel, M.-C.; Chen, S.-H. *Physica B* **1997**, *234*−*236*, 370−374.
(49) Chen, S.-H.; Gallo, P.; Sciortino, F.; Tartaglia, P. *Phys. Rev. E* **1997**, *56* (4), 4231−4243.
(50) Borodin, O.; Trouw, F.; Bedrov, D.; Smith, G. D. *J. Phys. Chem. B* **2002**, *106* (20), 5184−5193.
(51) Arab, M.; Bougeard, D.; Smirnov, K. S. *Phys. Chem. Chem. Phys.* **2003**, *5*, 4699−4707.
(52) Arab, M.; Bougeard, D.; Smirnov, K. S. *Phys. Chem. Chem. Phys.* **2004**, *6*, 2446−2453.
(53) Sposito, G.; Prost, R. *Chem. Rev.* **1982**, *82*, 553−573.
(54) Lechner, R. E. *Solid State Ionics* **1995**, *77*, 280−286.
(55) Hall, P. L.; Ross, D. K. *Mol. Phys.* **1978**, *36*, 1549−1554.
(56) Hall, P. L.; Ross, D. K. *Mol. Phys.* **1981**, *42*, 673−682.